ISSN 0915-633X

NATIONAL INSTITUTE FOR FUSION SCIENCE

Analysis of Oversized Sliding Waveguide by Mode Matching and Multi-Mode Network Theory

K. Ohkubo, S. Kubo, H. Idei, T. Shimozuma, Y. Yoshimura,
F. Leuterer, M. Sato and Y. Takita

(Received - June 26, 2000)

NIFS-671 Dec. 2000

RESEARCH REPORT
NIFS Series

TOKI, JAPAN

ANALYSIS OF OVERSIZED SLIDING WAVEGUIDE BY MODE MATCHING AND MULTI-MODE NETWORK THEORY

K. Ohkubo*, S. Kubo*, H. Idei*, T. Shimozuma*,
Y. Yoshimura*, F. Leuterer**, M. Sato*, and Y. Takita*

* *National Institute for Fusion Science*
** *Max-Planck Institut für Plasmaphysik*

Abstract : Transmission and reflection coefficients of HE_{11} hybrid modes in the sliding waveguide are discussed on the basis of mode matching method and multi-mode network theory. The sliding waveguide is composed of the corrugated waveguide with 88.9 mmϕ and the smooth-wall waveguide with 110 mmϕ in inner diameter. It is confirmed that the decrease in power of $< 0.2\%$ at 84 GHz is obtained for 2 cm in gap of the sliding waveguide. At the sliding length near multi-half-wavelength in vacuum, transmission and reflection powers in the sliding waveguide change slightly, because the very small amount of standing wave of higher-order TE or TM modes is produced resonantly.

Key Words : *mode-matching method, multi-mode network theory, sliding waveguide, corrugated waveguide, coupling, transmission line, electron cyclotron heating*

1 Introduction

There has been considerable interest in plasma production, heating and current drive of fusion-oriented plasmas by high-power electron cyclotron waves in the range of millimeter wave [1-7]. In a fusion-relevant devices such as ITER [8], the research and development of electron cyclotron heating is being continued. The electron cyclotron heating system is mainly composed of gyrotrons, oversized transmission lines and antennas. It is well-known that alignment of an oversized waveguide transmission line is important because deformation due to thermal expansion, its own weight or misalignment produces spurious modes and reduces transmission efficiency . When the injection port for electron cyclotron heating power is completely fixed, no change in transmission length and direction arises. In a super-conducting device, vacuum vessel is slightly displaced during cooling-down phase of coils. In tokamaks, the plasma disruption produces vibration of vacuum vessel. To absorb movement and vibration, waveguide bellows or quasi-optical components are used. Combination of miter-bends with sliding waveguides is able to absorb perpendicular two-dimensional displacement on the waveguide-axis and change in the length. In the large helical device [1], sliding waveguides are installed from the first cooling phase onwards. In this paper, a theoretical analysis of a sliding waveguide is given on the base of the mode-matching method and multi-mode network techniques. Transmission and reflection characteristics including higher-order modes excited in the component and formation of standing wave are described.

2 Theoretical Analysis and Discussion

A sliding waveguide which consists of movable and sleeve waveguides is shown in Figure 1(a). Two corrugated waveguides with the inner diameter $2a = 88.9$ mm are inserted into the smooth-wall waveguide which has an inner diameter of $2b = 110$ mm. The sliding surface is coated with MoS_2 and sealed with a silicon O-ring. Main purpose to analyze this transmission element is to make an estimation of the mode-conversion loss and the mode trapping in the waveguide gap. By using an electromagnetic (EM) analysis in the mode-matching method, we take reflection from the discontinuous junction planes into consideration. The complex amplitude of eigen waveguide modes in both transmission and reflection can then be calculated. As shown in Figure 1(b), waveguide diameter at the junction of sliding section increases or decreases in connection with injecting direction of EM wave. Hereafter, we label this waveguide (junction) as the up-step or the down-step

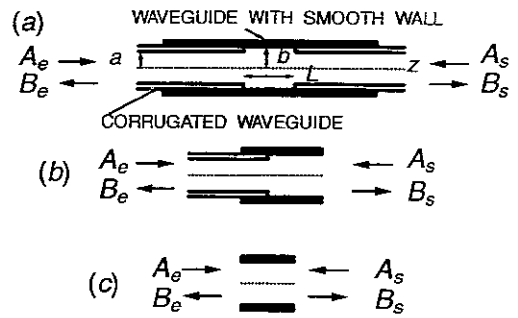

Figure 1: (a) The sliding waveguide with gap length L (b) the up-step (down-step) waveguide and (c) the smooth-wall waveguide. Here, A and B are incident and reflected complex amplitudes. The entrance and exit ports are defined as e and s in suffix.

waveguide (junction). At the junction surface, the tangential EM fields should be continuous. Equations satisfying the boundary condition at the junction plane of the down-step waveguide are given by

$$\boldsymbol{e}_0^+ + \sum_n^\infty C_n \boldsymbol{e}_n^- = \sum_m^\infty D_m \boldsymbol{E}_m^+ \qquad (1)$$

$$\boldsymbol{h}_0^+ + \sum_n^\infty C_n \boldsymbol{h}_n^- = \sum_m^\infty D_m \boldsymbol{H}_m^+ + 2\boldsymbol{h}_0^+ H(a) \qquad (2)$$

where, all the vectors signify their tangential components and relations of $\boldsymbol{e}_n^+ = \boldsymbol{e}_n^-$ and $\boldsymbol{h}_n^+ = -\boldsymbol{h}_n^-$ are satisfied from power flow. Here, m, n are mode number , $(+,-)$ is the traveling direction of each mode. EM-fields $(\boldsymbol{e}_0^+, \boldsymbol{h}_0^+)$, $(\boldsymbol{e}_n^-, \boldsymbol{h}_n^-)$ are the incident and reflected modes in the input waveguide and $(\boldsymbol{E}_m^+, \boldsymbol{H}_m^+)$ transmitted mode to the output waveguide, respectively. In Eq. 2, the term which includes the Heviside function H is the induced field at the ring-shaped metallic end of the corrugated waveguide when the EM-wave in the smooth-wall waveguide is injected into the corrugated waveguide. As for the junction of the up-step waveguide, the term $2\boldsymbol{h}_0^+ H(a)$ is excluded. Here, we take N HE, EH modes in the input and output corrugated waveguides and also N TE and TM modes in the smooth-wall waveguide. To determine the coefficients C_n and D_m, Γ_N for the least square method is introduced:

$$\Gamma_N = \frac{\int_S |\boldsymbol{e}_0^+ + \sum_n^{2N} C_n \boldsymbol{e}_n^- - \sum_m^{2N} D_m \boldsymbol{E}_m^+|^2 dS}{\int_S |\boldsymbol{e}_0^+|^2 dS} + \frac{\int_S |\boldsymbol{h}_0^+ + \sum_n^{2N} C_n \boldsymbol{h}_n^- - \sum_m^{2N} D_m \boldsymbol{H}_m^+ - 2\boldsymbol{h}_0^+ H(a)|^2 dS}{\int_S |\boldsymbol{h}_0^+|^2 dS} \qquad (3)$$

If $N = \infty$, Γ_∞ is equal to zero. In finite mode number N,

$$\frac{\partial \Gamma_N}{\partial C_i^*} = 0 \qquad (4)$$

$$\frac{\partial \Gamma_N}{\partial D_i^*} = 0 \qquad (5)$$

are satisfied in order to minimize Γ_N. Because C_i and D_i are complex value in general, we have $4N$ simultaneous linear equations:

$$Q_i = -\sum_j C_j T_{i,j} + \sum_j D_j U_{i,j} \qquad (6)$$

$$R_i = -\sum_j C_j V_{i,j} + \sum_j D_j W_{i,j} \qquad (7)$$

where,

$$T_{i,j} = \int \boldsymbol{e}_i^{-*} \cdot \boldsymbol{e}_j^- dS/K_e + \int \boldsymbol{h}_i^{-*} \cdot \boldsymbol{h}_j^- dS/K_h,$$

$$U_{i,j} = \int \boldsymbol{e}_i^{-*} \cdot \boldsymbol{E}_j^+ dS/K_e + \int \boldsymbol{h}_i^{-*} \cdot \boldsymbol{H}_j^+ dS/K_h,$$

$$V_{i,j} = \int \boldsymbol{E}_i^{+*} \cdot \boldsymbol{e}_j^- dS/K_e + \int \boldsymbol{H}_i^{+*} \cdot \boldsymbol{h}_j^- dS/K_h,$$

$$W_{i,j} = \int \boldsymbol{E}_i^{+*} \cdot \boldsymbol{E}_j^+ dS/K_e + \int \boldsymbol{H}_i^{+*} \cdot \boldsymbol{H}_j^+ dS/K_h,$$

$$Q_i = \int \boldsymbol{e}_i^{-*} \cdot \boldsymbol{e}_0^+ dS/K_e + \int \boldsymbol{h}_i^{-*} \cdot (\boldsymbol{h}_0^+ - 2\boldsymbol{h}_0^+ H(a)) dS/K_h,$$

$$R_i = \int \boldsymbol{E}_i^{+*} \cdot \boldsymbol{e}_0^+ dS/K_e + \int \boldsymbol{H}_i^{+*} \cdot (\boldsymbol{h}_0^+ - 2\boldsymbol{h}_0^+ H(a)) dS/K_h,$$

$$K_e = \int |\boldsymbol{e}_0^+|^2 dS, \text{ and } K_h = \int |\boldsymbol{h}_0^+|^2 dS.$$

Because EM fields $(\boldsymbol{e}_k^\pm, \boldsymbol{h}_k^\pm)$ $(\boldsymbol{E}_k^+, \boldsymbol{H}_k^+)$ on boundaries are is chosen to be real, $T_{i,j}$, $U_{i,j}$, $V_{i,j}$, $W_{i,j}$, Q_i and R_i are real and then coefficients C_j and D_j become real also. To carry out numerical integration, data files of two dimensional data, which are sampled at 64×64 points, are provided for all the modes. Here, the radius of corrugated waveguide is divided by 24 points.

The EM characteristics are analyzed by multimode network theory. A waveguide capable of propagating $2N$ modes is represented in term of $2N$ transmission lines with propagation constant β_q. In Figure 1(b) the up-step (down-step) waveguide with discontinuity has real two ports. Thus $4N$ virtual ports with TE_{1p}, TM_{1p}, HE_{1p} and EH_{1p} transmission lines for $p = 1 \sim N$ ($p = 2 \sim N+1$ for EH_{1p}) are considered owing to angular symmetric property. In the up-step (down-step) junctions, the incident, reflected and transmitted modes are related via the scattering matrix S as follows:

$$\begin{pmatrix} B_{e1} \\ B_{e2} \\ \cdots \\ \hline B_{s1} \\ B_{s2} \\ \cdots \end{pmatrix} = \left(\begin{array}{c|c} S_{11} & S_{12} \\ \hline S_{21} & S_{22} \end{array}\right) \begin{pmatrix} A_{e1} \\ A_{e2} \\ \cdots \\ \hline A_{s1} \\ A_{s2} \\ \cdots \end{pmatrix} \qquad (8)$$

where, the suffixes e and s indicate the entrance and exit ports, respectively. The incident and reflected hybrid modes are denoted by A_{eq} and B_{eq}, respectively. As for incident and reflected TE/TM modes, A_{sq} and B_{sq} are used:

$$A_{e1} = A_{eHE_{11}}, \ldots, A_{e(N+1)} = A_{eEH_{12}}, \ldots,$$

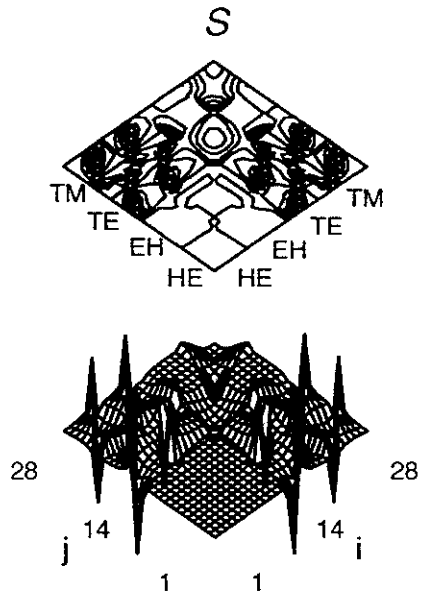

Figure 2: S-Matrix of the step waveguide for $N = 7$.

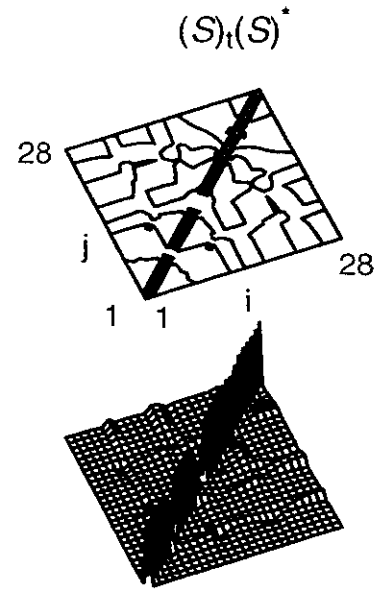

Figure 3: S_tS^* calculated from Figure 2. The matrix S is nearly unitary.

$$A_{s1} = A_{sTE_{11}}, \ldots, A_{s(N+1)} = A_{sTM_{11}}, \ldots,$$
$$B_{e1} = B_{eHE_{11}}, \ldots, B_{e(N+1)} = B_{eEH_{12}}, \ldots,$$
$$B_{s1} = B_{sTE_{11}}, \ldots, B_{s(N+1)} = B_{sTM_{11}}, \ldots.$$

Solutions C_j and D_j for various incident mode $(\boldsymbol{e}_0^+, \boldsymbol{h}_0^+)$ give S-matrix elements. In Figure 2, the contour and wire-frame plots of S-matrix for $N = 7$ at 84 GHz are shown. The choice of value N influences the absolute transmission power and mode trapping in gap of sliding waveguide. Because EM fields of higher-mode with large p in very large N are not represented exactly to the smallest details with the present sampling points, calculations of $T_{i,j}, U_{i,j}, V_{i,j}, W_{i,j}$, Q_i and R_i are truncated at $N = 7$. The S-matrix shows that injection of HE or EH mode to the smooth-wall waveguide into the up-step junction is almost completely transmitted as TE and TM modes: $S_{i,j} \simeq 0$ (for i and $j = 1 \sim 14$). As for injection of HE_{11} mode in the up-step waveguide, $S_{1,15} = -0.817$, $S_{1,16} = 0.227$, $S_{1,17} = 0.07$,.. and $S_{1,22} = -0.522$ which are coupling factors to TE_{11}, TE_{12}, TE_{13} and TM_{11} modes are obtained. It is noted that this values are different from well-known $S_{i,j}$ for $a = b$: $S_{1,15} = -0.919$, $S_{1,16} = 0.028$, $S_{1,22} = -0.3821$, and $S_{1,23} = -0.08$ for TE_{11}, TE_{12}, TM_{11} and TM_{12}. This result shows that the coupling of HE_{11} mode with the TE (TM) mode decreases (increases) when the diameter of smooth-wall waveguide becomes larger. On the other hand, TE and TM modes at the down-step junction are partially reflected by the end of the corrugated waveguide when these modes are injected into the corrugated waveguide: $S_{i,j} \neq 0$ (for i and $j = 15 \sim 28$). For example, in 28 modes of TE_{1p}, TM_{1p}, HE_{1p} and EH_{1p} for $p = 1 \sim 7$ ($p = 2 \sim 8$ for EH-mode), the calculation of S_tS^* shows that the off-diagonal terms are close to zero and that the diagonal terms except $(S_tS^*)_{66} = 0.82$, $(S_tS^*)_{77} = 0.07$, $(S_tS^*)_{12,12} = 0.84$, $(S_tS^*)_{13,13} = 0.08$, $(S_tS^*)_{14,14} = 0.03$ are close to unity as shown in Figure 3.

This attributes a truncation due to finite mode number and therefore the analysis is invalid for higher-mode injection with large p. For instance, the mode coupling of HE_{17} mode needs mainly (TE_{77}, TM_{77}) modes and requires more higher modes which is truncated. As for injection of a dominant HE_{11} mode or higher-mode with small p, the system almost conserves energy in spite of the finite mode number and therefore it is clear that the truncation has no significant impact on the analysis. When the sliding length L increases, the multi-reflection of TE and TM modes between step junctions excites more higher modes. In a scattering transfer description [9], (B_{sq}, A_{sq}) and (A_{eq}, B_{eq}) are related with scattering transfer matrices U and D for up-step and down-step waveguide components with L as follows:

$$\begin{pmatrix} B_{s1} \\ B_{s2} \\ \cdots \\ \hline A_{s1} \\ A_{s2} \\ \cdots \end{pmatrix} = \left(\begin{array}{c|c} \mathsf{U}_{11} & \mathsf{U}_{12} \\ \hline \mathsf{U}_{21} & \mathsf{U}_{22} \end{array}\right) \begin{pmatrix} A_{e1} \\ A_{e2} \\ \cdots \\ \hline B_{e1} \\ B_{e2} \\ \cdots \end{pmatrix} \tag{9}$$

$$\begin{pmatrix} B_{e1} \\ B_{e2} \\ \cdots \\ \hline A_{e1} \\ A_{e2} \\ \cdots \end{pmatrix} = \left(\begin{array}{c|c} \mathsf{D}_{11} & \mathsf{D}_{12} \\ \hline \mathsf{D}_{21} & \mathsf{D}_{22} \end{array}\right) \begin{pmatrix} A_{s1} \\ A_{s2} \\ \cdots \\ \hline B_{s1} \\ B_{s2} \\ \cdots \end{pmatrix} \tag{10}$$

where, $\mathsf{U}_{11} = \mathsf{S}_{21} - \mathsf{S}_{22}\mathsf{S}_{12}^{-1}\mathsf{S}_{11}$, $\mathsf{U}_{12} = \mathsf{S}_{22}\mathsf{S}_{12}^{-1}$,

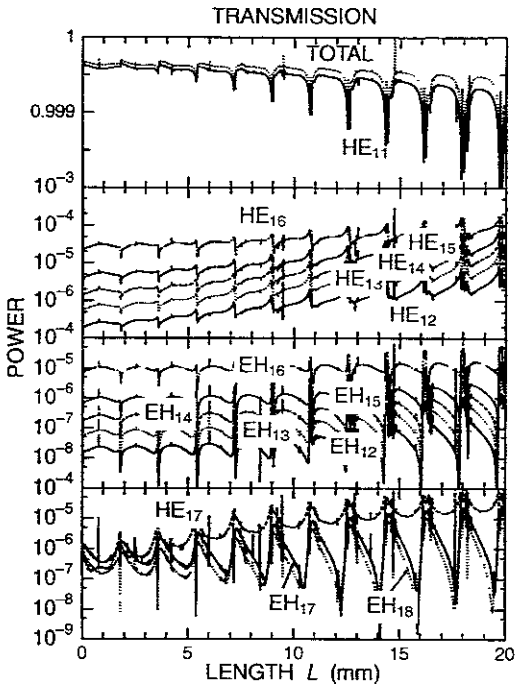

Figure 4: The transmitted power in the output of sliding waveguide as a function of the sliding length L.

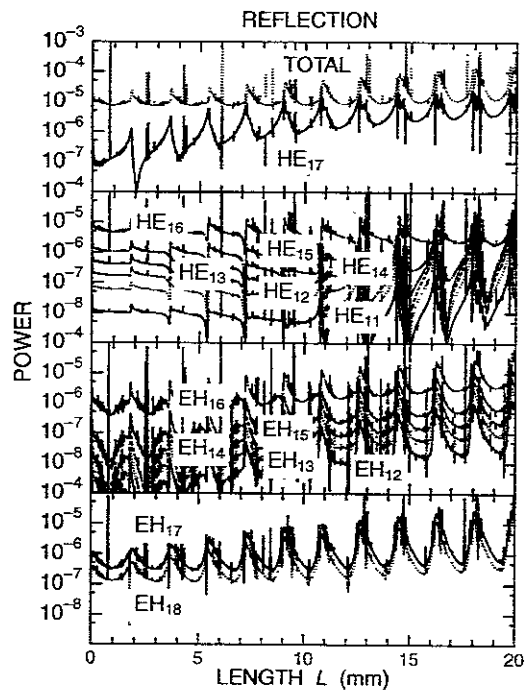

Figure 5: The reflected power in the input of sliding waveguide as a function of the sliding length L.

$\mathsf{U}_{21} = -\mathsf{S}_{12}^{-1}\mathsf{S}_{11}$, $\mathsf{U}_{22} = \mathsf{S}_{12}^{-1}$, $\mathsf{D}_{11} = \mathsf{S}_{12} - \mathsf{S}_{11}\mathsf{S}_{21}^{-1}\mathsf{S}_{22}$, $\mathsf{D}_{12} = \mathsf{S}_{11}\mathsf{S}_{21}^{-1}$, $\mathsf{D}_{21} = -\mathsf{S}_{21}^{-1}\mathsf{S}_{22}$, and $\mathsf{D}_{22} = \mathsf{S}_{21}^{-1}$. For the straight waveguide component of Figure 1(c), scattering transfer matrix F is given by

$$\begin{pmatrix} B_{s1} \\ B_{s2} \\ \hline \dots \\ A_{s1} \\ A_{s2} \\ \dots \end{pmatrix} = \left(\begin{array}{c|c} \mathsf{F}_{11} & 0 \\ \hline 0 & \mathsf{F}_{22} \end{array}\right) \begin{pmatrix} A_{e1} \\ A_{e2} \\ \hline \dots \\ B_{e1} \\ B_{e2} \\ \dots \end{pmatrix} \qquad (11)$$

where,

$$(\ \mathsf{F}_{11}\ ) = \begin{pmatrix} e^{-j\theta_1} & 0 & \dots & 0 \\ 0 & e^{-j\theta_2} & \dots & 0 \\ \vdots & \vdots & \vdots & 0 \\ 0 & 0 & 0 & e^{-j\theta_{2N}} \end{pmatrix} \qquad (12)$$

and

$$(\ \mathsf{F}_{22}\ ) = \begin{pmatrix} e^{j\theta_1} & 0 & \dots & 0 \\ 0 & e^{j\theta_2} & \dots & 0 \\ \vdots & \vdots & \vdots & 0 \\ 0 & 0 & 0 & e^{j\theta_{2N}} \end{pmatrix}. \qquad (13)$$

where, F_{11} and F_{22} are matrices related with $+z$ and $-z$ propagating mode. The value θ_q is the phase angle of TE (for $q \leq N$) and TM (for $q > N$) modes and represented by $\theta_q = \beta_q L$ with propagation constant β_q. The sliding waveguide is given three cascaded networks with transfer matrices U, F and D.

Finally, the relation of output modes to input ones for the sliding waveguide is obtained by taking the ordered product of the individual matrices:

$$\begin{pmatrix} B_{s1} \\ B_{s2} \\ \hline \dots \\ A_{s1} \\ A_{s2} \\ \dots \end{pmatrix} = \mathsf{D}\,[\Re\mathsf{F} + \Im\mathsf{F}]\,\mathsf{U} \begin{pmatrix} A_{e1} \\ A_{e2} \\ \hline \dots \\ B_{e1} \\ B_{e2} \\ \dots \end{pmatrix}. \qquad (14)$$

Considering an HE_{11} mode of 84 GHz is injected into the sliding waveguide, transmitted modes B_{sq} and reflected modes B_{eq} are solved numerically as a function of the the sliding length L by substituting $A_{e1} = 1$, $A_{eq} = 0$ (for $q \neq 1$), and $A_{sq} = 0$. In the case of an HE_{12} injection, B_{sq} and B_{eq} are obtained by $A_{e2} = 1$, $A_{eq} = 0$ (for $q \neq 2$) and $A_{sq} = 0$. In Figure 4 and Figure 5, transmitted and reflected power fractions of HE_{1p} and EH_{1p} modes are plotted as a function of sliding length L for mode number of $N = 7$ when only the HE_{11} mode is injected into the sliding waveguide. It is confirmed that transmission power of HE_{11} mode at $L = 0$ becomes close to unity when N increases: this value for $N = 5, 6, 7, ..$ is 0.9994, 0.9996, 0.9997, ... Because phase difference between TE_{11} and TM_{11} modes increases with L, power fraction of transmitted HE_{11} mode, which is composition of TE_{11} and TM_{11} modes, decreases. Typically, for $L = 2$ cm, the transmission loss of HE_{11} mode is less than 0.2%, which includes resonant dips. With increasing L, periodic changes in

the transmission and the reflection modes are observed: the depth of the troughs increases and the period is almost a half-wavelength in vacuum $\lambda_0/2$. To show the periodicity and the evolution of dips in detail, in Figure 6, the transmitted HE_{11} power to the output of sliding waveguide is shown as a function of L. Here, each curve is displaced vertically by three half-wavelengths in vacuum. The number n_p shows the period between $L = (n_p - 1)\lambda_0/2$ and $n_p\lambda_0/2$. As discussed later, the depth and width of the first (second) dip results from resonances of TM_{12}, $(TE_{13}, TE_{11}, TE_{15}, \ldots)$ modes. Near the first and second half-wavelength periods the transmitted power increases, and then resonant dips and the shelf appear.

In Figure 7, the transmitted power HE_{11} for various N around $L = 9\lambda_0/2$ are shown as a function of L. Figures 7 (a) to (g) corresponds to $N = 1$ to 7, respectively. For reference, the positions of ninth half waveguide-lengths of TE and TM modes are plotted by vertical dotted lines. As N increases, the transmitted power increases gradually, and dips appear in the region indicated by the vertical lines. The first and second dips arise at $N \geq 3$ and $N \geq 6$, respectively. The dips originate in formation of a partial standing wave of higher-order TE and TM modes with large p. By substituting the calculated complex amplitudes B_{eq} of the reflected HE and EH modes to the input waveguide and the given incident complex amplitudes ($A_{e1} = 1$ and $A_{eq} = 0$ for $q \neq 1$) in Eq. 9, $+z$ and $-z$ propagating modes amplitudes A_{sq} and B_{sq}, with TE and TM modes at the junction plane are obtained.

As shown in Figure 8, the total transmitted power ((+z propagating power) − (−z propagating power)) at the up-step junction remains constant and the total +z propagating power at the same junction

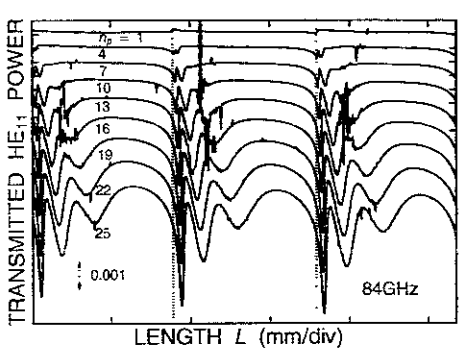

Figure 6: The transmitted HE_{11} power. The curves are displaced in each case by every three half-wavelength in vacuum. The vertical value of the top horizontal line is unity. The curves are displaced downwards in each case by one vertical division, which corresponds to 0.001. The number n_p shows the period between $L = (n_p - 1)\lambda_0/2$ and $n_p\lambda_0/2$.

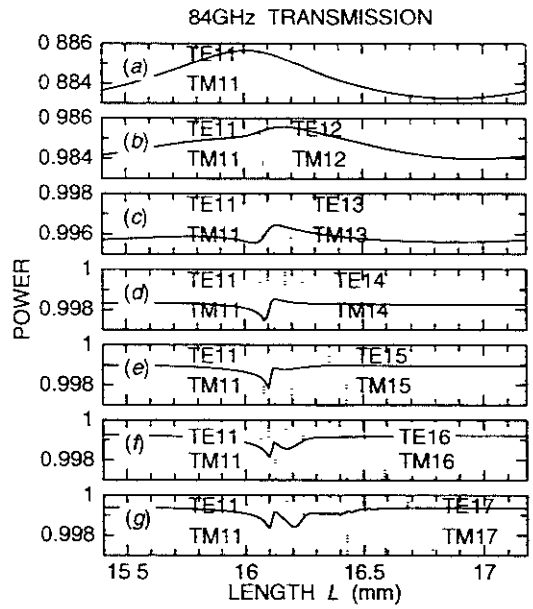

Figure 7: The transmitted HE_{11} power around $L = 9\lambda_0/2 = 16.06$ mm: figure (a) to (g) corresponds to $N = 1$ to 7. Vertical dotted lines indicate locations which are equal to ninth half waveguide-length of TE and TM modes.

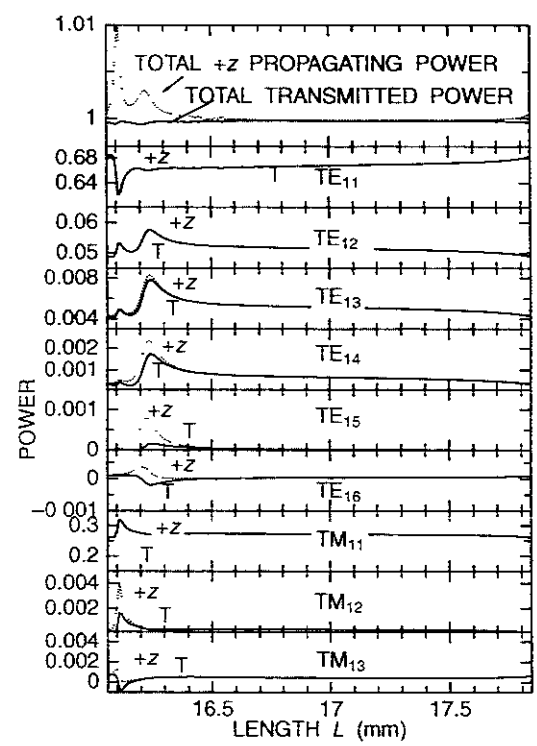

Figure 8: The transmitted and +z propagating powers in the smooth wall waveguide as a function of L. Powers of +z propagation and transmission for down-step junction are denoted by +z and T.

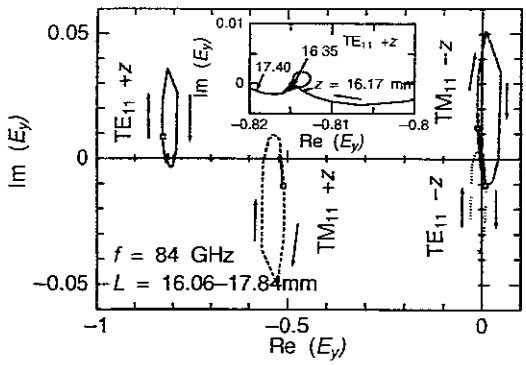

Figure 9: The polar plot of complex amplitude in $+z$ and $-z$ propagating waves at the up-step junction.

shows two peaks of which values are more than unity. This attributes the increase in total $-z$ propagating power. Although TE_{11}, TE_{12} and TM_{11} modes are almost traveling wave, TM_{12}, TE_{13} TE_{14} and TE_{15} modes are partial standing waves in the sliding waveguide. At the special length near every half-wavelength period, trapped TM_{12} and (TE_{13}, TE_{14} and TE_{15}) modes generate first and second dips of the transmitted HE_{11} as shown in Figure 7.

By comparing those results with that shown in Figure 7, it seems that cascade decay to higher-mode with large p by low reflection of higher-mode with small p produces standing wave. With relation to Figure 8, the E_y of $+z$ and $-z$ propagating TE_{11} and TM_{11} modes as typical example at the up-step junction is polar-plotted in Figure 9. From the point of $L = 16.06$ mm denoted by the square, the trajectories rotate clockwise rapidly and move slowly near the real axis when L increases. This behavior is also seen for higher TE and TM modes. A large rotation with an imaginary part relates with the dip formation mentioned previously. To obtain field pattern $|E_y|$ and $|H_x|$ at any position z in the smooth-wall waveguide with given L, complex fraction of $\pm z$ propagating modes can be calculated as follows:

$$\begin{pmatrix} B_{s1} \\ B_{s2} \\ \cdots \\ \hline A_{s1} \\ A_{s2} \\ \cdots \end{pmatrix} = [\Re\mathsf{F} + \Im\mathsf{F}]_{\theta_q=\beta_q z}\ \mathsf{U} \begin{pmatrix} A_{e1} \\ A_{e2} \\ \cdots \\ \hline B_{e1} \\ B_{e2} \\ \cdots \end{pmatrix}. \quad (15)$$

where θ_q in F is redefined as $\theta_q = \beta_q z$. The total field $|E_y|$ and $|H_x|$ are obtained as the sum of TE and TM mode pattern with weighting factor of fraction calculated. In Figures 10 and 11, the normalized electric fields in the smooth-wall waveguide for special lengths of $L = 16.10$ and 16.21 mm are plotted as a function of z. In the peripheral region, standing wave patterns with nine peaks due to higher modes of TM in Figure 10 and TE in Figure 11 are observed clearly due to small amplitude of low-order mode.

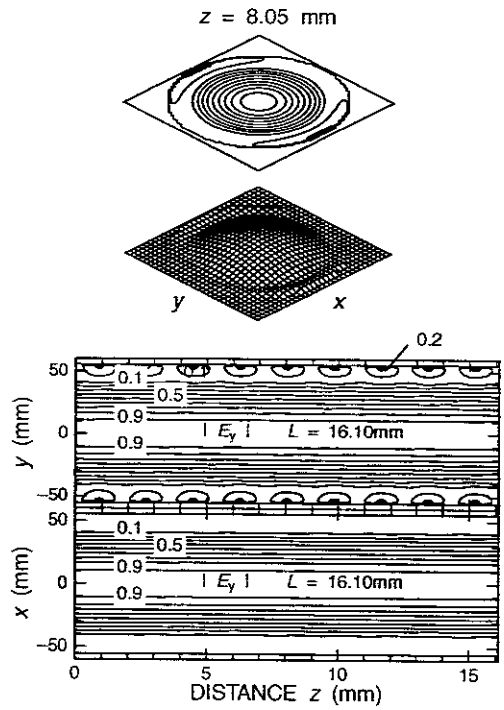

Figure 10: Normalized $|E_y|$ in the smooth-wall waveguide for $L = 16.10$ mm of the first dip in Figure 8.

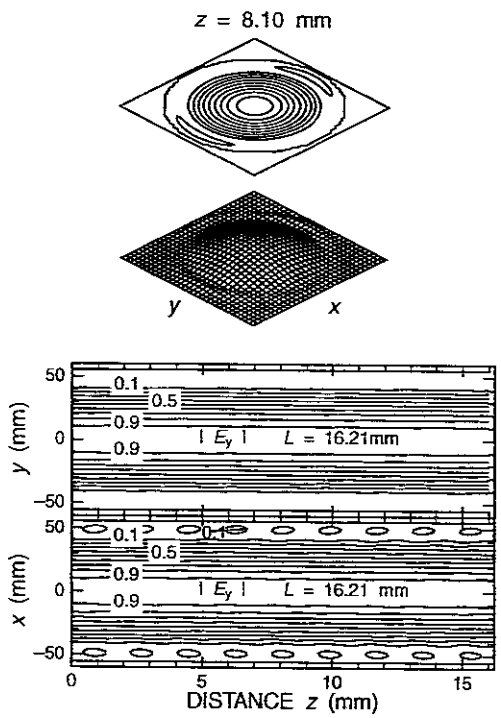

Figure 11: Normalized $|E_y|$ in the smooth-wall waveguide for $L = 16.21$mm of the second dip in Figure 8.

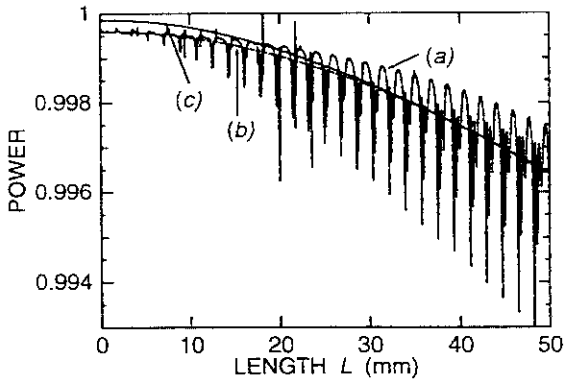

Figure 12: Comparison of the transmitted HE_{11} mode: (a) the sliding waveguide with $2a = 88.9$ mm and $2b = 110$ mm (b) with absorbers on the end of the corrugated waveguide are added and (c) when the straight smooth-wall waveguide with $2b = 88.9$ mm is inserted in the gap.

In the central region nearly traveling wave patterns, which is similar to the HE_{11} mode, are also observed in both figures. Apparently the standing wave is produced by reflection between the the ends of waveguide when they are inserted.

When the EM absorbing material is to be placed in front of the ends of corrugated waveguide, no multi-reflection arises as shown in Figure 12(b). When a straight waveguide with the same inner diameter ($2a = 2b = 88.9$ mm) is inserted in stead of the smooth-wall waveguide in sliding waveguide, the multi-reflection also ceases as shown in Figure 12(c). Because the wavenumber difference $\Delta\beta$ between TE_{11} and TM_{11} mode in $2a = 2b = 88.9$ mm is larger than that in $2a = 88.9$ mm and $2b = 110$ mm, the mode-conversion loss increases.

In all the cases the total mode-conversion loss is less than 0.2% at $L = 2$ cm. The similar calculated results at 168 GHz are also obtained [1]: the periodic behavior of transmitted and reflected modes is also observed and the mode-conversion loss decreases to $< 0.1\%$ at $L = 2$ cm.

3 Summary

A theoretical analysis of sliding waveguide with $2b = 110$ mmϕ, which connects corrugated waveguides with $2a = 88.9$ mmϕ, has been performed by a combination of mode-matching and scattering matrix techniques. The results are as follows: (1) small amount of higher-order modes in reflection and transmission is excited and that an 84GHz-HE_{11} mode is transmitted with the loss of $< 0.2\%$ including the resonant effect at the sliding length $L = 2$ cm: (2) at a special length near the multi-half-wavelength, mode-conversion loss is enhanced due to the presence of the standing wave in the gap. It can be expected that resonant dips are smoothed down when corrugated waveguides with rounded out or inclined ends in the sliding waveguide are adopted

Acknowledgments

The authors would like to thank Drs. O. Motojima and M. Fujiwara for his continuing encouragement.

References

[1] K. Ohkubo, S. Kubo, T. Shimozuma, H. Idei, M Sato et al.: to be published in *Proc. of 4th Int. Conf. on Strong Microwave in Plasmas*, Nizhny Novgorod 1999.

[2] T.C. Luce, Y.R. Lin-Liu, J.M. Lohr, C.C. Petty, R. Prater et al.: *Proc. of 17th IAEA Fusion Energy Conference*, **1**, 611, Yokohama (IAEA, Vienna 1999).

[3] F. Ryter, F. Leuterer, M. Beckmann, H. Brinkshulte, R. Brückner et al.: to be published in *Proc. of 4th Int. Conf. on Strong Microwave in Plasmas* , Nizhny Novgorod 1999.

[4] V. Erckmann, V. Gasparino, H.P. Laqua, H. Massberg et al: *Proc. of 17th IAEA Fusion Energy Conference*, **2**, 639, Yokohama (IAEA, Vienna 1999).

[5] Z.A. Pietrzyk, A. Pochelon, T.P. Goodman, M.A. Henderson, J.-P. Hogge et al.: Nucl. Fusion, **39**, 587 (1999).

[6] S. Cirant, P. Buratti, G. Braqcco, O. Tudisco, M. Zerbiri et al.: *Proc. of 17th IAEA Fusion Energy Conference*, **2**, 647, Yokohama (IAEA, Vienna 1999).

[7] R.F.G. Meulenbroeks, M.R. deBaars, M.N.A. Beurskens, H.J. deBlank, B.H. Deng et al.: Phys of Plasmas **6**, 3898, 1999.

[8] G. Bosia, M. Makowski, P. Froissard, R. Koch, P. Prins et al.: Proc. of 17th IAEA Fusion Energy Conference, **3**, 1021, Yokohama (IAEA, Vienna 1999)

[9] M Sucher and J. Fox: *Handbook of Microwave Measurements* vol. 1, 328 (Polythechnic Press, 1963).

Recent Issues of NIFS Series

NIFS-657 M Sasao, S Murakami, M Isobe, A V Krasilnikov, S Iiduka, K Itoh N Nakajima, M Osakabe, K Saito,T Seki, Y.Takeiri, T Watari, N Ashikawa , P deVaries, M Emoto, H Funaba, M Goto, K Ida, H Idei, K Ikeda, S Inagaki, N Inoue, S Kado, O Kaneko, K.Kawahata, K.Khlopenkov, T.Kobuchi , A Komori, S Kubo R Kumazawa, S Masuzaki, T Minami, J Miyazawa, T Morisaki, S Morita, S Muto, T Mutoh, Y Nagayama, Y Nakamura, H Nakanishi, K.Narihara K Nishimura, N Noda, T Notake, Y Liang , S Ohdachi, N Ohyabu, Y Oka, T Ozaki, R O Pavlichenko, B J Peterson, A Sagara, S Sakakibara, R Sakamoto, H Sasao4, K Sato, M Sato, T Shimozuma, M Shoji, H Suzuki, M Takechi, N Tamura, K Tanaka, K Toi, T Tokuzawa, Y Torii, K Tsumori, H Yamada, I Yamada, S Yamaguchi, S Yamamoto, M Yokoyama, Y Yoshimura, K Y Watanabe and O Motojima,
Study of Energetic Ion Transport in the Large Helical Device Sep 2000
(IAEA-CN-77/EX9/1)

NIFS-658 B J Peterson, Y Nakamura, K Yamazaki, N.Noda, J Rice, Y Takeiri, M Goto, K Narihara, K Tanaka, K Sato, S Masuzaki, S Sakakibara, K Ida, H Funaba, M Shoji M Osakabe, M Sato, Yuhong Xu, T Kobuchi, N Ashikawa, P deVries, M Emoto, H Idei, K Ikeda, S Inagaki, N Inoue, M.Isobe, S Kado, K Khlopenkov, S Kubo, R Kumazawa, T Minami, J Miyazawa, T Morisaki, S Murakami, S Muto, T Mutoh, Y Nagayama, H Nakanishi, K.Nishimura, T.Notake, Y Liang, S Ohdachi, Y Oka, T.Ozaki, R O Pavlichenko, A Sagara, K Saito, R Sakamoto, H Sasao, M Sasao, T Seki, T Shimozuma, H Suzuki, M Takechi, N Tamura, K Toi, T Tokuzawa, Y Torii, K.Tsumori, I Yamada, S.Yamaguchi, S Yamamoto, M Yokoyama, Y Yoshimura, K Y Watanabe, T Watari, K Kawahata, O Kaneko, N Ohyabu, H Yamada, A Komori, S Sudo, O Motojima
Impurity transport induced oscillations in LHD Sep 2000
(IAEA-CN-77/EXP5/27)

NIFS-659 T Satow, S Imagawa, N Yanagi, K Takahata, T Mito, S Yamada, H Chikaraishi, A Nishimura, I Ohtake, Y Nakamura, S. Satoh, O Motojima,
Achieved Capability of the Superconducting Magnet system for the Large Helical Device Sep 2000
(IAEA-CN-77/FTP1/15)

NIFS-660 T Watari, T Mutoh, R Kumazawa, T Seki, K Saito, Y Torii , Y P Zhao , D. Hartmann , H Idei, S Kubo, K Ohkubo, M. Sato, T Shimozuma, Y Yoshimura, K Ikeda, O Kaneko, Y Oka, M Osakabe, Y. Takeiri, K Tsumori, N.Ashikawa , P C deVries, M Emoto, A.Fukuyama , H. Funaba, M Goto, K Ida, S Inagaki, N Inoue, M Isobe, K Itoh, S Kado, K Kawahata, T Kobuchi, K.Khlopenkov, A Komori, A Krasilnikov , Y Liang,S Masuzaki, K Matsuoka, T Minami, J Miyazawa, T Morisaki, S. Morita, S Murakami, S Muto, Y. Nagayama, Y Nakamura, H Nakanishi, K Narihara, K. Nishimura, N. Noda, A. T.Notake, S Ohdachi, N Ohyabu, H Okada , M Okamoto, T Ozaki, R O Pavlichenko, B J Peterson, A Sagara, S Sakakibara, R. Sakamoto, H Sasao, M. Sasao, K Sato, S Satoh, T Satow, M. Shoji, S Sudo, H Suzuki, M Takechi, N Tamura ,S Tanahashi, K Tanaka, K Toi, T Tokuzawa, K Y Watanabe, T Watanabe, H Yamada, I. Yamada, S Yamaguchi, S Yamamoto, K Yamazaki, M Yokoyama, Y Hamada, O Motojima, M. Fujiwara,
The Performance of ICRF Heated Plasmas in LHD Sep 2000
(IAEA-CN-77/EX8/4)

NIFS-661 K Yamazaki, K. Y. Watanabe, A Sagara, H. Yamada, S Sakakibara, K Narihara, K. Tanaka, M Osakabe, K Nishimura, O Motojima, M Fujiwara, the LHD Group.
Helical Reactor Design Studies Based on New Confinement Scalings Sep 2000
(IAEA-CN-77/ FTP 2/12)

NIFS-662 T Hayashi, N Mizuguchi, H Miura and T Sato
Dynamics of Relaxation Phenomena in Spherical Tokamak Sep 2000
(IAEA-CN-77THP2/13)

NIFS-663 H. Nakamura and T Sato, H Kambe and K Sawada and T Saiki,
Design and Optimization of Tapered Structure of Near-field Fiber Probe Based on FDTD Simulation Oct. 2000

NIFS-664 N Nakajima,
Three Dimensional Ideal MHD Stability Analysis in $L=2$ Heliotron Systems Oct 2000

NIFS-665 S Fujiwara and T Sato,
Structure Formation of a Single Polymer Chain I Growth of trans Domains Nov 2000

NIFS-666 S Kida,
Vortical Structure of Turbulence Nov. 2000

NIFS-667 H Nakamura, S Fujiwara and T Sato,
Rigidity of Orientationally Ordered Domains of Short Chain Molecules: Nov 2000

NIFS-668 T Mutoh, R Kumazawa, T Seki, K Saito, Y Torii, F Shimpo, G Nomura, T Watari, D A. Hartmann, M. Yokota, K. Akaishi, N. Ashikawa, P deVries, M. Emoto, H. Funaba, M Goto, K Ida, H Idei, K. Ikeda, S. Inagaki, N. Inoue, M. Isobe, O Kaneko, K Kawahata, A Komori, T Kobuchi, S Kubo, S Masuzaki, T Morisaki, S Morita, J Miyazawa, S Murakami, T Minami, S Muto, Y. Nagayama, Y Nakamura, H Nakanishi, K Narihara, N. Noda, K Nishimura, K. Ohkubo, N Ohyabu, S Ohdachi, Y Oka, M. Osakabe, T Ozaki, B.J. Peterson, A Sagara, N Sato, S Sakakibara, R Sakamoto, H Sasao, M. Sasao, M Sato, T Shimozuma, M Shoji, S. Sudo, H Suzuki, Y. Takeiri, K Tanaka, K. Toi, T Tokuzawa, K Tsumori, K Y. Watanabe, T Watanabe, H Yamada, I. Yamada, S Yamaguchi, K Yamazaki, M Yokoyama, Y Yoshimura, Y Hamada, O Motojima, M Fujiwara,
Fast- and Slow-Wave Heating of Ion Cyclotron Range of Frequencies in the Large Helical Device Nov 2000

NIFS-669 K Mima M S Jovanovic Y Sentoku, Z-M Sheng, M.M Skoric and T Sato,
Stimulated Photon Cascade and Condensate in Relativistic Laser-plasma Interaction Nov 2000

NIFS-670 L. Hadzievski, M M. Skoric and T Sato,
On Origin and Dynamics of the Discrete NLS Equation Nov 2000

NIFS-671 K Ohkubo, S. Kubo, H Idei, T Shimozuma, Y Yoshimura, F Leuterer, M Sato and Y Takita,
Analysis of Oversized Sliding Waveguide by Mode Matching and Multi-Mode Network Theory, Dec. 2000